Am J Transl Res 2026;18(8):7420-7437
www.ajtr.org /ISSN:1943-8141/AJTR0174336

Original Article

Effectiveness and multidimensional mechanisms of close-to-bone needling in knee osteoarthritis: a randomized controlled trial

Yumei Lu[1], Huiying Wu[1], Nini Fu[2], Qian Su[1], Qi Zeng[1], Yifan He[1], Yi Ren[1]

[1]Department of Rehabilitation Medicine, Hanzhong Hospital of Traditional Chinese Medicine, Hanzhong 723102, Shaanxi, China; [2]Department of Acupuncture, Tongliang Hospital of Traditional Chinese Medicine, Chongqing 402560, China

Received May 28, 2026; Accepted July 16, 2026; Epub August 15, 2026; Published August 30, 2026

Abstract: Objectives: To evaluate the clinical efficacy of close-to-bone needling (CBN) in patients with knee osteoarthritis (KOA) and to explore its underlying mechanisms. Methods: Seventy patients with KOA were randomized to receive either CBN (n=35) or oral celecoxib (Drug Group, DG, n=35) for a 4-week intervention period, followed by a 2-week follow-up. Additionally, 35 healthy controls (HC) were enrolled. Clinical outcomes were assessed using the Western Ontario and McMaster Universities Osteoarthritis Index (WOMAC), the Index of Severity for Osteoarthritis of the Knee (ISOA), and the 36-Item Short Form Health Survey (SF-36). Structural alterations were evaluated by magnetic resonance imaging (MRI)-based Whole-Organ Magnetic Resonance Imaging Score (WORMS) and musculoskeletal ultrasound. Molecular changes were assessed by quantifying plasma and synovial fluid levels of miR-140, miR-30, interleukin-1β (IL-1β), and tumor necrosis factor-α (TNF-α). Neural correlates were assessed via resting-state electroencephalography (EEG), including spectral power analysis and graph-theoretical analysis of brain network characteristics. Results: Compared with the DG group, the CBN group showed significantly greater overall clinical efficacy at 6 weeks ($P<0.05$), with greater improvements in WOMAC, ISOA, and SF-36 scores, as well as greater reductions in cartilage degeneration, synovial thickening, and joint effusion ($P<0.05$). Furthermore, CBN produced stronger modulatory effects on miR-140, miR-30, IL-1β, and TNF-α levels ($P<0.05$). EEG analysis revealed reduced Delta and Theta power, increased Alpha, Beta, and Gamma power in frontoparietal regions, and normalization of abnormal prefrontal connectivity patterns in the Theta and Gamma frequency bands ($P<0.05$). Conclusion: CBN represents an effective non-pharmacological intervention for KOA, with advantages over celecoxib in symptom relief, joint structure improvement, molecular regulation, and central neural normalization. The proposed "brain-molecule-clinic" assessment framework provides multidimensional evidence supporting the potential mechanisms of acupuncture-based interventions in KOA.

Keywords: Knee osteoarthritis, close-to-bone needling, electroencephalography, microRNA, inflammatory cytokines

Introduction

Osteoarthritis (OA) is a prevalent degenerative joint disorder characterized by progressive cartilage degradation, synovial inflammation, and changes in subchondral bone structure, ultimately leading to pain, swelling, and joint stiffness. OA represents one of the leading causes of disability and chronic pain worldwide [1]. Knee osteoarthritis (KOA) accounts for approximately 60.8% of global disability burden attributed to OA [2]. Epidemiological projections indicate that the number of KOA cases will increase by approximately 74.9% by 2050 compared within 2020 [3]. In China, the prevalence of symptomatic KOA is estimated at 8.1%, with KOA-associated years lived with disability (YLD) reaching 1.97 million person-years [4], imposing a considerable burden on both society and individuals. The pathogenesis of KOA involves a complex interplay of mechanical wear, inflammatory responses, and metabolic dysregulation within articular cartilage and subchondral bone, ultimately leading to progressive cartilage degradation. Established risk factors for KOA include advanced age (particularly >50

https://doi.org/10.62347/NGZG8291

years), obesity (body mass index [BMI] >28 kg/m^2), previous knee trauma, prolonged occupational activities involving kneeling or squatting, and a family history of OA.

Current management strategies for KOA, as outlined in clinical guidelines, focus primarily aim to alleviate symptoms and preserve joint function; however, no available treatment has yet achieved a fundamental cure [5]. Nonsteroidal anti-inflammatory drugs (NSAIDs) are widely used because of their convenience and relatively rapid analgesic effects. However, long-term NSAID administration is limited by potential adverse effects, including gastric ulcers, gastrointestinal bleeding, and renal impairment [6]. Surgical intervention is generally reserved for severe KOA, particularly those with severe joint-space narrowing and persistent pain refractory to conservative therapies [7]. Therefore, the development of safe and effective non-pharmacological interventions for pain relief and disease control remains an urgent clinical need. Exercise therapy and weight management are established examples of non-pharmacological interventions that can be safely implemented over long periods and are associated with fewer systemic side effects than pharmacological treatments, making them suitable for patients with early- to moderate-stage KOA.

Acupuncture, a practice with a history of more than 3,000 years in China and other Asia regions, has gained increasing global recognition and has been included in the WHO International Classification of Diseases (ICD-11), as a treatment modality for chronic pain [8]. In traditional Chinese medicine (TCM), KOA is classified within the categories of "bone impediment" and "bi syndrome" [9]. Close-to-bone needling (CBN), a specialized acupuncture technique for treating KOA, has been recorded documented in classical Chinese medical literature, including the *Huangdi Neijing*.

The concept of acupuncture neuroimaging was first introduced in 2000 and has since evolved into an interdisciplinary research field integrating acupuncture, neuroscience, and neuroimaging technologies. Acupuncture stimulation has been shown to modulate central nervous system activity through peripheral inputs [10]. Electroencephalography (EEG) provides a non-invasive approach for assessing cortical electrical activity and has been used to study brain functional states and evaluate neurophysiological responses to acupuncture stimulation [11].

At the molecular level, microRNAs (miRNAs) regulate gene expression through post-transcriptional mechanisms. By combining the systemic regulatory effects of acupuncture with the gene-regulatory functions of microRNAs, the concept of a "molecular network regulation" mechanism has been proposed to provide explanations for the disease-modifying effects of acupuncture. miR-140 is highly expressed in healthy cartilage but is down-regulated during OA progression, where it regulates cartilage degradation-related targets, including ADAMTS-5 and IGFBP-5 [12]. In contrast, the miR-30 family is upregulated in OA and may promote OA progression by targeting the ETS-related gene (ERG) and reducing aggrecan expression [13].

In previous research, we applied the CBN technique in a rabbit model of KOA to investigate its potential peripheral mechanisms in repairing articular cartilage. Specifically, the CBN method can repair the cartilage extracellular matrix homeostasis by positively regulating the type II collagen-DDR2-MMP13 signaling pathway [14], promote articular cartilage synthesis by suppressing Runx2 and ColX expression [15], and inhibit chondrocyte apoptosis while enhancing chondrocyte proliferation by through regulation of Caspase-3, Bax, and proliferating cell nuclear antigen (PCNA) expression [16]. Mechanistically, CBN stimulation at specific acupoints near bone surfaces may induce local mechanical signals that activate discoidin domain receptor 2 (DDR2) in chondrocytes, thereby regulating MMP13 expression through downstream MAPK/ERK signaling and restoring the balance between cartilage matrix synthesis and degradation [17, 18].

However, the clinical mechanisms underlying CBN treatment and objective evidence supporting its efficacy remain insufficiently elucidated. Therefore, this study was designed to investigate the clinical efficacy and potential mechanisms of CBN in patients with KOA. In this study, we established an integrated evaluation framework comprising brain functional network analysis (EEG), molecular biomarker detection (miRNAs), and clinical efficacy evaluation (scales,

imaging, and ultrasound), providing a comprehensive approach for investigating the therapeutic mechanisms of acupuncture in KOA.

Methods

Study design and participants

This prospective, randomized, controlled study employed a 1:1 allocation ratio between treatment groups. The intervention period lasted 4 weeks with a 2-week follow-up period. The study was conducted in accordance with the Standards for Reporting Interventions in Clinical Trials of Acupuncture (STRICTA) and the Consolidated Standards of Reporting Trials (CONSORT) guidelines [19]. Participants were assessed at baseline, 4 weeks, and 6 weeks post-treatment initiation.

This study was conducted in accordance with the Declaration of Helsinki and its subsequent amendments. Ethical approval was obtained from the Ethics Committee of Hanzhong Hospital of Traditional Chinese Medicine (Ethical code: HZZYY2022001) prior to patient enrollment. All participants provided written informed consent after receiving both written and oral explanations of the study procedures, risks, and their rights to withdraw at any time. The trial was registered with the International Traditional Medicine Clinical Trial Registry (Registration number: ITMCTR2025001693). The ethics approval documentation is provided as a supplementary file.

This exploratory study aimed to compare the clinical efficacy of CBN and celecoxib in improving pain and functional outcomes in KOA patients over a 4-week intervention and 2-week follow-up. Additionally, the study sought to examine the underlying mechanism of CBN in KOA treatment. Given the exploratory nature of this study, a formal sample size calculation was not performed. Based on clinical feasibility and experience, a sample size of 70 subjects (35 in each cohort) was deemed adequate to achieve the objectives of this pilot investigation.

Seventy patients with KOA were recruited from the Department of Rehabilitation Medicine at Hanzhong Hospital of Traditional Chinese Medicine between January 2022 and December 2023 and randomly assigned in a 1:1 ratio to either the CBN group or the drug treatment group (DG; celecoxib). Additionally, 35 healthy controls (HC), matched for age, sex, and body mass index (BMI) to the case group using the paired matching method, were recruited from relatives or caregivers of patients in the same department. The TCM diagnostic criteria for KOA were based on the "liver-kidney deficiency pattern" within the category of "Bone Bi Syndrome" as outlined in the *Criteria for Diagnosis and Therapeutic Effects of Diseases and Syndromes in Traditional Chinese Medicine* (T/CACM 1227-2019), while Western diagnostic criteria were based on the *Chinese Guidelines for the Diagnosis and Treatment of Osteoarthritis (2021 edition).* According to these guidelines, KOA severity was classified radiographically using the Kellgren-Lawrence (K/L) grading system (grades 0-IV) and clinically by symptom duration, pain severity, and functional limitation, with grades II and III representing moderate disease suitable for non-surgical interventions.

Inclusion criteria: (1) diagnosis of KOA according to the aforementioned TCM and Western medical criteria; (2) age between 40 and 70 years; (3) BMI was ≤30 kg/m^2; (4) radiographic K/L grade II or III, with grade II defined as definite osteophyte formation with possible joint-space narrowing and grade III defined as multiple moderate osteophytes, definite joint-space narrowing, mild sclerosis, and possible bone deformity; (5) Brief Pain Inventory (BPI) score >2, Mini-Mental State Examination (MMSE) score ≥24, and Beck Depression Inventory (BDI) score <14; and (6) provision of informed consent and willingness to participate voluntarily.

Exclusion criteria: (1) bleeding tendency or hemorrhagic disorders; (2) knee surgery within the previous 6 months or intra-articular glucocorticoid administration within the previous 3 months; (3) primary or secondary muscle diseases; (4) pre-existing severe knee deformity; (5) a history of knee trauma resulting in joint instability or lower-limb malalignment; (6) severe cardiovascular or cerebrovascular diseases, major musculoskeletal disorders, or organ failure; and (7) mental disorders, inability to independently complete study procedures, or poor compliance.

Participants were withdrawn from the study under the following conditions: (1) Voluntary

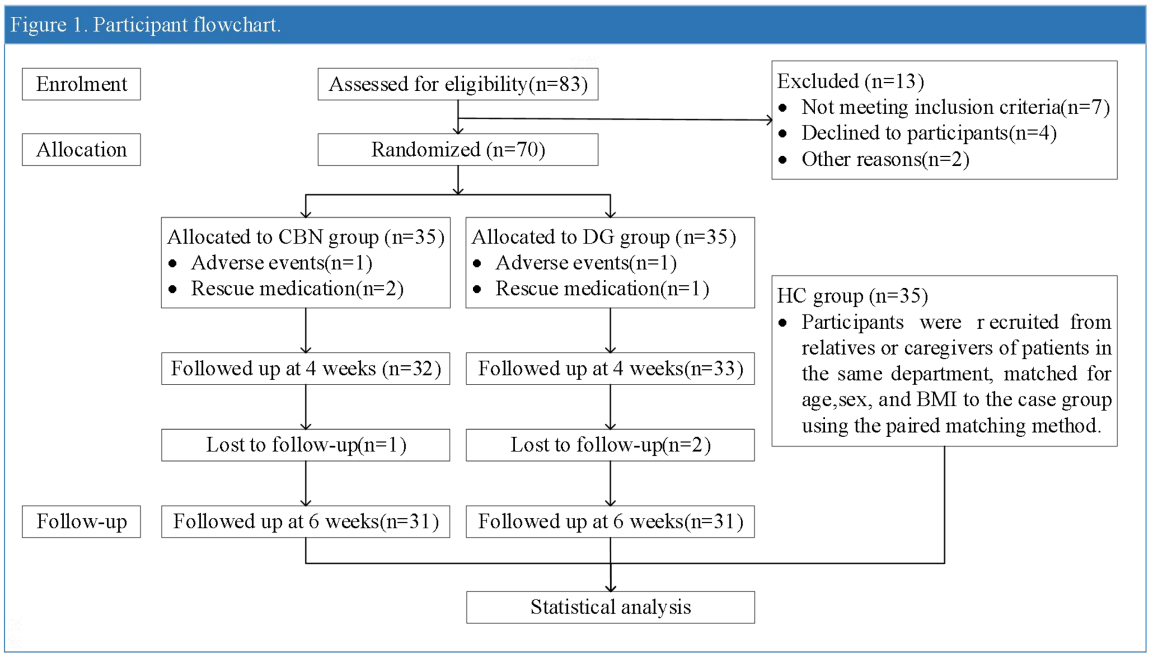

Figure 1. Flowchart for participant enrollment.

withdrawal; (2) Failure to complete the treatment or follow-up assessments; (3) Pregnancy; (4) Disease progression or death; (5) Occurrence of severe adverse events (AEs); (6) Use of prohibited drugs during treatment.

Randomization and allocation concealment

A computer-generated randomization sequence (1-70) was created using SPSS 25.0. And then used to assign patients to the CBN or DG groups at a 1:1 ratio. Allocation concealment was ensured using sequentially numbered, opaque, sealed envelopes (SNOSE). An independent staff member who was not involved in participant recruitment, treatment administration, or outcome assessment prepared and sealed the envelopes according to the randomization sequence. After enrollment and completion of baseline assessments, the corresponding envelope was opened to reveal the assigned intervention. The allocation information was then provided to the treatment personnel responsible for intervention delivery.

Blinding

This was a single-blind study in which outcome assessors and data analysts were blinded to treatment allocation; however, blinding of participants and acupuncturists was not feasible because of the nature of the interventions. To minimize potential performance bias, participants received treatment in separate rooms and were not informed of the intervention received by other participants.

Study treatment

All patients with KOA underwent comprehensive clinical assessments. Demographic and clinical characteristics, including age, sex, marital status, employment status, education level, pain duration (months), and KOA severity stage, were collected and recorded at baseline. Radiographic severity was evaluated according to the Kellgren-Lawrence (K/L) grading system based on knee radiographs. The study flow chart is presented in **Figure 1**.

All acupuncture practices in the CBN group were performed by a licensed physician with 8 years of clinical experience and formal acupuncture training. Disposable sterile steel needles (Huatuo brand; Suzhou Medical Appliance Co., Ltd., Jiangsu, China) were used. EX-LE4 (Neixiyan), EX-LE5 (Waixiyan), SP9 (Yinlingquan), ST36 (Zusanli) and ST34 (Liangqiu) were selected as the acupuncture points according to the Guidelines for the Nomen-

clature and Location of Acupuncture Points (National Standard of the People's Republic of China: GB/T 12346-2006) [20].

Acupuncture intervention was performed according to a standardized protocol as follows: (1) For EX-LE4 (Neixiyan) and EX-LE5 (Waixiyan), a 30 mm × 0.25 mm filiform needle was inserted obliquely toward the joint cavity to a depth of approximately 20 mm until contacting with the bone surface, followed by withdrawal of 1-2 mm to minimize direct periosteal stimulation; (2) For SP9 (Yinlingquan) and ST36 (Zusanli), a 30 mm × 0.25 mm needle was inserted perpendicularly adjacent to the tibial margin and advanced along the bone cortex to a depth of about 20-25 mm; (3) For ST34 (Liangqiu), a 45 mm × 0.25 mm needle was inserted obliquely towards the femur until reaching the periosteum, followed by gentle needle manipulation toward SP10 (Xuehai) at a depth of approximately 30-35 mm. After needle insertion at all acupoints, manual manipulation including lifting, thrusting, and rotating techniques was applied uniformly for 1 minute at each point to elicit deqi sensation. The needles were retained in place for 20 minutes per session. The acupuncture treatment schedule consisted of 6 consecutive treatment days, followed by a 1-day rest period, with each 7-day period considered one treatment cycle. A total of four cycles (28 days of active treatment) were completed.

Patients in the DG group received oral celecoxib capsules (Celebrex; Pfizer Pharmaceuticals Co., Ltd.; 0.2 g per capsule, batch number: S52334) once daily. The administration schedule was identical to that of the CBN group, consisting of 6 consecutive treatment days, followed by a 1-day rest period for a total of four cycles (28 days in total).

No treatment was applied to the HC group. Healthy controls underwent baseline clinical assessment and were included only for comparison of clinical and biological measurements.

Clinical efficacy and safety assessment

Clinical efficacy was evaluated according to the Criteria for Diagnosis and Therapeutic Effect Evaluation of TCM Diseases and Syndromes (ZY/T 001.9-1994). The efficacy criteria were as follows: (1) Markedly effective: complete relief of knee joint pain and swelling, along with restoration of normal joint mobility; (2) Effective: partial improvement in knee joint pain and swelling, with increased joint mobility; (3) Ineffective: no significant reduction in knee joint pain, swelling, or restricted joint mobility. The overall response rate was calculated as the sum of participants classified as markedly effective or effective.

(1) Western Ontario and McMaster Universities Osteoarthritis Index (WOMAC): The WOMAC score was used to measure the extent of KOA-related symptoms and functional impairment in both the CBN and DG groups before and after intervention. It consists of three aspects: pain (5 items), stiffness (2 items), and physical function (17 items). Higher scores indicate more severe knee joint damage [21]. (2) Index of Severity for Osteoarthritis of the Knee (ISOA) [22]: The ISOA was used to evaluate KOA severity and functional limitations based on morning stiffness, joint swelling, resting pain, exercise-induced pain, squatting/knee flexion ability, and maximum walking distance. A higher total score indicates more severe limb dysfunction. (3) 36-Item Short Form Health Survey (SF-36): The SF-36 was applied to assess health-related quality of life (HRQoL) [23], covering 36 items across eight domains: physical functioning, social functioning, physical role functioning, emotional role function, mental health, vitality, bodily pain, and general health. Higher total scores indicate better health status and quality of life.

All subjects were instructed to report any adverse events (AEs) occurring throughout the treatment period. AEs were documented and evaluated by clinicians. Acupuncture-related AEs included local bleeding, bruising, pallor, sweating, dizziness, syncope, intolerable needle pain, and persistent post-treatment needle sensation. Drug-related AEs mainly included nausea, vomiting, or gastrointestinal bleeding.

Throughout the study period, all patients were prohibited from using additional NSAIDs outside the study protocol. For participants experiencing severe uncontrolled pain, celecoxib (0.2 g orally) was provided as a temporary rescue medication. Patients requiring rescue medication were withdrawn from the trial, and the reasons for medication use and withdrawal was documented in the case report forms (CRFs).

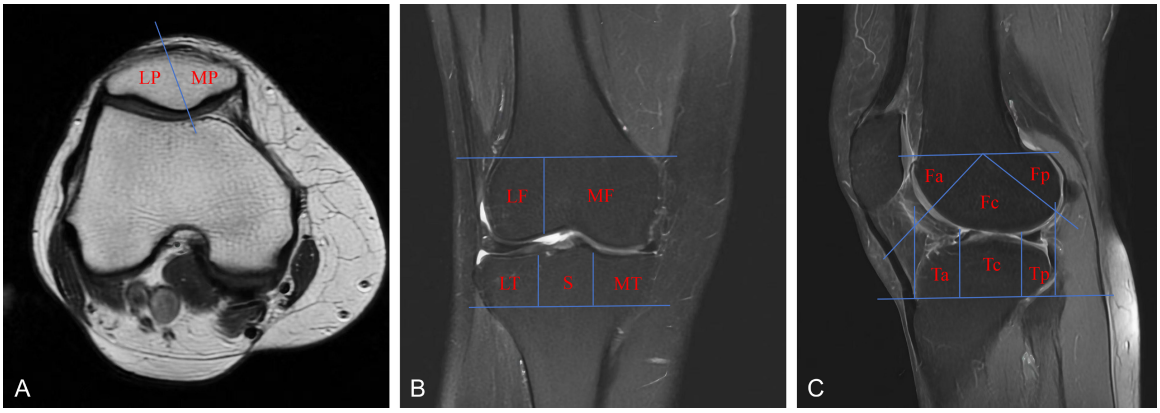

Figure 2. Division of the knee joint area. A: The patellar region was categorized into the Medial Patella (MP) and Lateral Patella (LP) based on the patellar crest. B: The femoral condyle was similarly classified into the Medial Femoral Condyle (MF) and Lateral Femoral Condyle (LF) according to the lateral condyle of the femur. The Sub-tibial region (S) of the tibial plateau, which experiences articular cartilage loss, was divided into the Medial Tibial Plateau (MT) and Lateral Tibial Plateau (LT), with S serving as the boundary. C: The femoral regions were further subdivided into Anterior Femoral (Fa), Central Femoral (Fc), and Posterior Femoral (Fp) at designated points. Additionally, the tibial plateau was segmented into Tibial Anterior (Ta), Tibial Central (Tc), and Tibial Posterior (Tp) in the sagittal orientation.

Imaging assessment

MRI evaluation was performed using the Whole-Organ Magnetic Resonance Imaging Score (WORMS), a semi-quantitative scoring system widely used for comprehensive assessment of knee joint structural abnormalities. The purpose of WORMS assessment was to objectively quantify cartilage morphological changes across 15 predefined knee regions and enable standardized longitudinal comparison of structural alterations between treatment groups. In the patellar region, the medial patella (MP) and lateral patella (LP) were defined according to the patellar ridge. In the femoral compartment, the medial femoral condyle (MF) and the lateral femoral condyle (LF) were delineated according to the anatomical division of the femoral condyles. In the tibial compartment, the tibial plateau was divided into medial tibial plateau (MT) and lateral tibial plateau (LT) regions, with S serving as the boundary. Subdivision of the femoral and tibial region was refined in the sagittal plane, including the anterior femoral (Fa), central femoral (Fc), posterior femoral (Fp), anterior tibial (Ta), central tibial (Tc), and posterior tibial (Tp) regions (**Figure 2**). Cartilage morphological changes in each region was scored graded on a semi-quantitative scale from 0 to 6 according to the WORMS criteria. The total score was calculated by summing the scores across all assessed regions, with higher scores indicating more severe structural abnormalities.

Ultrasound was performed to evaluate knee joint effusion and synovial membrane thickness before and after treatment. Patients in CBN and DG groups were positioned supine with the affected limb elevated by 10° to facilitate fluid accumulation within the suprapatellar recess. A Toshiba SSA-680A ultrasound system was used to scan the suprapatellar bursa. Joint effusion was defined as an anechoic area exceeding 1 mm within the joint capsule. Subsequently, the probe was used to displace fluid, and the maximum synovial thickness was measured. Synovial membrane thickness was assessed according to the Walther classification criteria, and knee joint effusion was graded according to the Agostino classification criteria.

Mechanistic assessment

Peripheral venous blood samples (5 mL) were collected from patients in CBN and DG groups before and after treatment following an overnight fast. Samples were centrifuged at 2500 rpm (approximately 1000×g) for 10 minutes to isolate plasma supernatant. Synovial fluid samples (500 μL) were obtained from the knee joint through aspiration and centrifuged at 3000 rpm (approximately 1800×g) for 10 min to collect supernatant. All supernatants under-

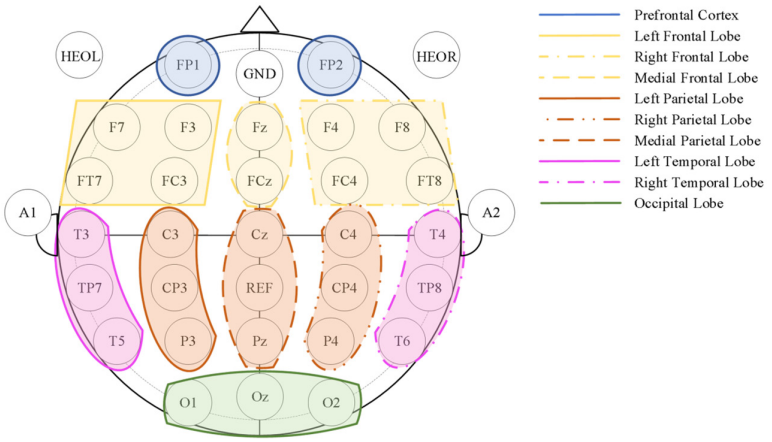

Figure 3. Brain region division for electroencephalography signal collection.

went a secondary centrifugation at 12,000 rpm (approximately 13,800×g) for 10 min at 4°C. The resulting supernatants were aliquoted and stored at -80°C until further analysis. The expression levels of miR-140 and miR-30 in plasma and synovial fluid were quantified using fluorescent quantitative reverse transcription polymerase chain reaction (qPCR) (Shanghai ZJ Bio-Tech Co., Ltd.; Code: 20183401705). Relative miRNA expression levels were calculated using the $2^{-\Delta\Delta Ct}$ method.

The concentrations of IL-1β and TNF-α in synovial fluid were determined using enzyme-linked immunosorbent assay (ELISA) (Shanghai Enzyme-linked Biotechnology Co., Ltd.; Code: ml106733 and ml002095). Reference ranges were defined as <50 pg/mL for IL-1β and <30 fmol/mL for TNF-α according to the manufacturer's specifications.

Resting-state EEG recordings were performed before and after treatment to non-invasively assess cortical oscillatory activity and functional brain network alterations associated with KOA-related chronic pain, and to investigate the potential modulatory effects of CBN treatment on aberrant central neural activity. EEG signals were acquired pre- and post-treatment stages using a 64-lead EEG cap positioned according to the international 10-20 electrode placement system. A 0.9% sodium chloride solution was used as the conductive medium. A noisy-signal-amplifying circuit (ZhenTec NT1) was connected to the electrode, and a low-noise preamplifier was used. Electrode impedance was maintained below 10 kΩ. Subjects were instructed to remain relaxed in a resting state with eyes closed during a 5-minute EEG recording period. EEG signals were sampled at 1,000 Hz, and environmental noise was recorded for subsequent analysis.

MATLAB 2021b was used to preprocess EEG data as follows: (1) notch filtering at 50 Hz; (2) sixth-order Butterworth band-pass filtering between 1 and 30 Hz; (3) exclusion of irrelevant or malfunctioning electrodes; (4) independent component analysis (ICA) for removal of ocular and other artifact components; (5) visual inspection for signal drift and residual artifacts, followed by linear interpolation; (6) average referencing across channels; and (7) segmentation into 2-second epochs, with epochs containing amplitudes exceeding 75 μV excluded from further analysis.

After preprocessing, EEG signals were decomposed into five frequency bands as follows: Delta (1-4 Hz), Theta (4-8 Hz), Alpha (8-15 Hz), Beta (15-30 Hz), and Gamma (30-45 Hz). Electrode regions were grouped into the following cortical areas (**Figure 3**): prefrontal cortex (FP1, FP2), left frontal lobe (F3, FC3, F7, FT7), right frontal lobe (F4, FC4, F8, FT8), medial frontal lobe (Fz, FCz), left parietal lobe (C3, CP3, P3), right parietal lobe (C4, CP4, P4), medial parietal lobe (Cz, REF, Pz), left temporal lobe (T3, TP7, T5), right temporal lobe (T4, TP8, T6), and occipital lobe (Oz, O1, O2).

Relative EEG power was calculated by dividing the power of individual frequency bands by the total power in the frequency range of 1-45 Hz using Fast Fourier Transform (FFT). Power spectral density (PSD) was estimated using the Welch method with a 1-second time window and 50% overlap. Relative power for each frequency band was calculated as the ratio of the power within a specific frequency range to the total power from 1 to 45 Hz:

$$RePower(f_1, f_2) = \frac{Power(f_1, f_2)}{Power(1, 45)}$$

where *Power (f1, f2)* denotes the spectral power within the target frequency band, and

Table 1. Demographic and baseline characteristics of included participants

Characteristic	CBN group (n=31)	DG group (n=31)	HC group (n=34)	*P*-value
Demographics				
Age (years)	56.76±13.78	56.84±11.78	57.01±12.21	0.818
Sex (male/female, n)	18/13	16/15	17/17	0.781
Body mass index (Kg/m^2)	23.02±3.51	22.82±4.78	23.22±3.13	0.816
Educational background (years)	8.23±3.99	8.78±4.01	9.37±6.37	0.715
Smoking (yes/no, n)	10/21	11/20	12/22	0.924
Drinking (yes/no, n)	5/26	5/26	6/28	0.831
Handedness (left/right, n)	3/28	4/27	6/28	0.868
Clinical Characteristics				
Duration (years)	3.54±1.12	3.01±1.58	-	0.761
Side (left/right/bilateral, n)	12/14/5	13/13/5	-	0.564
Kellgren-Lawrence grade (II/III, n)	10/21	11/20	-	0.911

CBN: Close-to-Bone Needing; DG: drug; HC: health control; n: number of cases.

Power (1, 45) represents the total power between 1 and 45 Hz. Relative power values were used to characterize frequency-specific cortical activity during resting-state conditions.

For brain network analysis, 30 channels were defined as network nodes. Initially, the weight phase lag index (wPLI) was used to quantify functional connectivity between the channels, which measures phase synchronization while reducing the influence of volume conduction effects. The calculation was defined as:

$$wPLI = \frac{|\langle \Im(X) \rangle|}{\langle |\Im(X)| \rangle} = \frac{|\langle |\Im(X)| \cdot sign(\Im(X)) \rangle|}{\langle |\Im(X)| \rangle}$$

where $\Im(X)$ represents the imaginary component of the cross-spectrum between $X_{(t)}$ and $Y_{(t)}$, $0 \leq wPLI \leq 1$, where a value of 0 indicated asynchrony and a value of 1 indicated synchronization. An association matrix was then created based on these values. Weak correlations were removed using a 20% network sparsity threshold. Four key graph theory indicators were selected: global clustering coefficient (GCC), mean degree (MD), network density (ND), and global efficiency (GE).

Statistical analyses

Statistical analyses were performed using MATLAB 2020a software. Categorical variables were presented as [n (%)] and analyzed using the Chi-square test. The distribution of continuous variables was assessed using the Kolmogorov-Smirnov test. Data conforming to normal distribution were expressed as mean ± standard deviation (SD), and comparisons between two independent groups were conducted using the independent-samples t-test, while paired t-tests were used for within-group comparisons before and after intervention. Non-normally distributed continuous variables were expressed as median (QL, QU) and analyzed using the Wilcoxon rank-sum test. The threshold for statistical significance was set at $P<0.05$. Spearman's rank-order correlation analysis was performed to evaluate associations between continuous variables.

Results

Baseline characteristics

A total of 70 participants with KOA were randomly assigned to the CBN (n=35) or the DG (n=35) groups. During the study period, four participants (11.4%) in the CBN group, four (11.4%) in the DG group, and one (2.8%) in the HC group withdrew from the study. Consequently, 31 participants (88.6%) in the CBN group, 31 (88.6%) in the DG group, and 34 (97.2%) in the HC group were included in the per-protocol analysis. Baseline characteristics and clinical characteristics of the groups are summarized in **Table 1**. No significant differences were observed between the CBN and DG groups in baseline demographic or clinical characteristics, clinical parameters, or other measured variables ($P>0.05$).

Table 2. Comparison of the total response rate between CBN and DG groups

Time	Group	n	Markedly effective (n)	Effective (n)	Ineffective (n)	Total effectiveness rate (n, %)	*P*-value
6 weeks	CBN group	31	16	12	3	28 (90.32)	0.026
	DG group	31	12	10	9	22 (70.96)	

CBN: Close-to-Bone Needing; DG: drug; n: number of cases.

Table 3. Comparison of the WOMAC scores between CBN and DG groups

CBN group	31	Pre-treatment	13.87±2.51	5.69±1.04	45.98±7.71	65.37±10.08
		6 weeks	8.51±2.71$^{*,\Delta}$	3.01±0.98$^{*,\Delta}$	30.18±6.15$^{*,\Delta}$	40.69±10.38$^{*,\Delta}$
DG group	31	Pre-treatment	13.69±2.54	5.29±1.31	44.91±6.31	66.19±11.21
		6 weeks	10.27±3.61*	4.21±0.87*	35.21±6.69*	50.26±11.37*

CBN: Close-to-Bone Needing; DG: drug; n: number of cases; WOMAC: Western Ontario and McMaster Universities Osteoarthritis Index. Compared with pre-treatment, $^{*}P<0.05$; compared with DG group at 6 weeks, $^{\Delta}P<0.05$.

Table 4. Comparison of the ISOA and SF-36 scores between CBN and DG groups

Group	n	Time	ISOA (points)	SF-36 (points)
CBN group	31	Pre-treatment	39.87±6.17	57.29±8.28
		6 weeks	68.78±6.41$^{*,\Delta}$	70.61±10.04$^{*,\Delta}$
DG group	31	Pre-treatment	40.27±5.91	56.69±9.27
		6 weeks	55.31±4.81*	65.81±10.91*

CBN: Close-to-Bone Needing; DG: drug; ISOA: Index of Severity for Osteoarthritis of the Knee. Compared with pre-treatment, $^{*}P<0.05$; compared with DG group at 6 weeks, $^{\Delta}P<0.05$.

Table 5. Comparison of cartilage morphology scores between CBN and DG groups

Group	n	Time	Cartilage Morphology Scores (points)
CBN group	31	Pre-treatment	2.98±1.31
		6 weeks	2.36±1.08$^{*,\Delta}$
DG group	31	Pre-treatment	2.87±1.95
		6 weeks	2.56±1.66*

CBN: Close-to-Bone Needing; DG: drug; Compared with pre-treatment, $^{*}P<0.05$; compared with DG group at 6 weeks, $^{\Delta}P<0.05$.

Clinical efficacy outcomes

The overall response rate in the CBN group at 6 weeks after treatment was significantly higher compared to the DG group ($P<0.05$; **Table 2**).

No significant differences were observed in baseline WOMAC, ISOA, or SF-36 scores between the CBN and DG groups ($P>0.05$). Both groups exhibited significant reductions in WOMAC scores at 6 weeks compared with baseline levels ($P<0.05$), with the CBN group displaying a notably greater decrease than the DG group ($P<0.05$; **Table 3**). Both groups demonstrated significant increases in ISOA and SF-36 scores after treatment compared with baseline values ($P<0.05$). Compared with the DG group, the CBN group exhibited significantly greater improvements in these scores after intervention ($P<0.05$; **Table 4**).

Imaging findings

No significant differences in MRI-based cartilage morphology scores were observed between the CBN and DG groups at baseline ($P>0.05$). After treatment, the scores decreased significantly in both groups, with the CBN group showing a notably lower score than the DG group (**Table 5**).

Similarly, no significant differences were observed in baseline synovial thickness or joint effusion between the two groups (both $P>0.05$). After treatment, both groups exhibited a significant reduction in synovial thickness and joint effusion at 6 weeks ($P<0.05$). Moreover, the CBN group showed greater reductions in these parameters compared with the DG group after treatment ($P<0.05$; **Table 6**).

Molecular biomarkers

No significant differences were observed in the baseline levels of miR-140 and miR-30 between

Table 6. Comparison of the synovial thickness and joint effusion between CBN and DG groups

Group	n	Time	Synovial Thickness (mm)	Joint Effusion (ml)
CBN group	31	Pre-treatment	4.10±1.45	5.26±2.14
		6 weeks	1.23±0.54$^{*,\Delta}$	2.37±1.56$^{*,\Delta}$
DG group	31	Pre-treatment	3.85±1.32	5.26±2.14
		6 weeks	1.64±0.48*	3.25±2.11*

CBN: Close-to-Bone Needing; DG: drug. Compared with pre-treatment, $^{*}P<0.05$; compared with DG group at 6 weeks, $^{\Delta}P<0.05$.

the CBN and DG groups ($P>0.05$). At 6 weeks post-treatment, both groups showed significantly increased miR-140 levels and decreased miR-30 levels, compared with baseline levels ($P<0.05$). Moreover, compared with the DG group, the CBN group exhibited a greater increase in miR-140 expression and a greater reduction in miR-30 expression at 6 weeks ($P<0.05$; **Table 7**).

Similarly, baseline IL-1β and TNF-α levels did not differ significantly between the CBN and DG groups ($P>0.05$). At post-treatment 6 weeks, both groups demonstrated significant reductions in IL-1β and TNF-α levels compared with baseline values ($P<0.05$). Furthermore, the reductions in inflammatory cytokine levels were significantly greater in the CBN group than the DG group ($P<0.05$; **Table 8**).

EEG spectral power analysis

In the Delta band (**Figure 4A**), after 6 weeks of treatment, relative power in the bilateral parietal, bilateral temporal, and occipital regions decreased significantly in both treatment groups compared with baseline values ($P<0.05$). Additionally, the CBN group showed significantly lower Delta power than the DG group after treatment ($P<0.05$). At baseline, patients in both treatment groups showed significantly higher Delta relative power in the right temporal and occipital regions compared with the HC group ($P<0.05$).

In the Theta band (**Figure 4B**), relative power decreased significantly in 10 brain regions after treatment in both treatment groups compared with baseline values ($P<0.05$). Additionally, the reduction was greater in the CBN group than in the DG group ($P<0.05$). At baseline, the CBN and DG groups demonstrated significantly higher Theta relative power than the HC group in all brain regions except for the prefrontal cortex region ($P<0.05$).

In the Alpha band (**Figure 4C**), after 6 weeks of treatment, significant increases in relative power were observed in the prefrontal cortex, medial frontal region, bilateral parietal regions, right temporal region, and occipital region of the patients in both groups ($P<0.05$). The CBN group exhibited significantly higher Alpha power than the DG group after treatment ($P<0.05$). At baseline, Alpha relative power in the prefrontal cortex, right parietal, and occipital regions was significantly lower in both treatment groups than in the HC group ($P<0.05$).

In the Beta band (**Figure 4D**), relative power significantly increased after 6 weeks of treatment in all assessed brain regions except for the prefrontal cortex in both CBN and DG groups, compared to baseline power ($P<0.05$). Additionally, the CBN group showed higher relative power than the DG group after treatment ($P<0.05$). At baseline, Beta relative power in the bilateral frontal, bilateral parietal, medial frontal, bilateral temporal, and occipital regions was significantly lower in both treatment groups compared to the HC group ($P<0.05$).

In the Gamma band (**Figure 4E**), significant increases in relative power after treatment were observed in the medial frontal and occipital regions in both CBN and DG groups compared with baseline levels ($P<0.05$). Additionally, the CBN group showed higher relative power than the DG group after treatment ($P<0.05$). At baseline, Gamma relative power in the medial frontal region was significantly lower in both the CBN and DG groups than in the HC group ($P<0.05$).

Representative scalp topographic maps of relative power changes before and after CBN treatment are shown in **Figure 5**. Compared with baseline, post-treatment map demonstrated decreased relative power in bilateral parietal and temporal regions, consistent with the group-level statistical findings.

Table 7. Comparison of miR-140 and miR-30 levels between CBN and DG groups

Group	n	Time	Blood		Synovial Fluid	
			miR-140	miR-30	miR-140	miR-30
CBN group	31	Pre-treatment	1.69±0.54	1.81±0.27	1.43±0.34	1.50±0.52
		6 weeks	2.68±0.71$^{*,\Delta}$	1.51±0.54$^{*,\Delta}$	2.42±0.31$^{*,\Delta}$	1.19±0.71$^{*,\Delta}$
DG group	31	Pre-treatment	1.71±0.36	1.83±0.26	1.41±0.42	1.51±0.54
		6 weeks	2.01±0.24*	1.61±0.76*	1.98±0.31*	1.28±0.67*

CBN: Close-to-Bone Needing; DG: drug. Compared with pre-treatment, $^{*}P<0.05$; compared with DG group at 6 weeks, $^{\Delta}P<0.05$.

Table 8. Comparison of IL-1β and TNF-α levels between CBN and DG groups

Group	n	Time	Blood		Synovial Fluid	
			IL-1β (pg/ml)	TNF-α (fmol/ml)	IL-1β (pg/ml)	TNF-α (fmol/ml)
CBN group	31	Pre-treatment	50.98±10.17	40.13±8.28	51.21±10.22	41.92±8.13
		6 weeks	22.78±9.51$^{*,\Delta}$	19.23±10.12$^{*,\Delta}$	22.06±9.31$^{*,\Delta}$	18.15±9.15$^{*,\Delta}$
DG group	31	Pre-treatment	51.23±10.13	41.23±10.01	50.21±11.11	42.76±10.23
		6 weeks	32.21±9.56*	24.27±9.32*	31.34±10.26*	24.18±9.12*

CBN: Close-to-Bone Needing; DG: drug; IL-1β: interleukin-1β; TNF-α: tumor necrosis factor-α. Compared with pre-treatment, $^{*}P<0.05$; compared with DG group at 6 weeks, $^{\Delta}P<0.05$.

Brain network topological analysis

Quantitative topological indicators demonstrated that following 6 weeks of treatment, the global clustering coefficient (GCC), mean degree (MD), and global efficiency (GE) of the Theta- and Gamma-band networks within the prefrontal cortex decreased significantly in both the CBN and DG groups compared with baseline levels ($P<0.05$). These values approached the levels observed in the HC group ($P>0.05$), with the CBN group exhibiting significantly lower values than the DG group after treatment ($P<0.05$). Before treatment, all four topological parameters of the Theta-band brain network in the prefrontal cortex were significantly higher in patients of the CBN and DG groups than in the HC group ($P<0.05$). After treatment, no significant differences were observed between the CBN and DG groups for these Theta-band prefrontal network parameters ($P>0.05$; **Figure 6**).

Correlation analysis

The change in Theta-band relative power in the left frontal region exhibited a positive correlation with the change in WOMAC score from baseline to post-treatment in the CBN group ($P<0.05$). Conversely, the change in Gamma-band relative power in the right frontal region demonstrated a negative correlation with the change in WOMAC score after treatment ($P<0.05$). The correlation results are presented in **Table 9** and **Figure 7**.

Discussion

KOA is a debilitating condition that significantly impairs patients' quality of life. CBN is an effective non-pharmacological intervention for KOA. In this study, we investigated the therapeutic effects of CBN for KOA and explored its potential mechanisms using a multidimensional framework integrating brain functional network analysis, molecular biomarkers, and clinical assessments.

The acupoints selected in this study included EX-LE4 (Neixiyan), EX-LE5 (Waixiyan), SP9 (Yinlingquan), ST34 (Liangqiu), and ST36 (Zusanli). EX-LE4 and EX-LE5 are located adjacent to the medial and lateral patellar ligaments, respectively. SP9 is a He-sea point of the Spleen Meridian that can help alleviate muscle atrophy and knee pain. ST34 and ST36 are frequently selected for alleviating knee swelling and pain. Previous studies have suggested that stimulation of these acupoints may regulate local circulation, modulate periarticular tissue function, and improve joint homeostasis [24-26].

In this study, CBN therapy significantly improved clinical outcomes, including reductions in WOMAC score, improvements in ISOA and

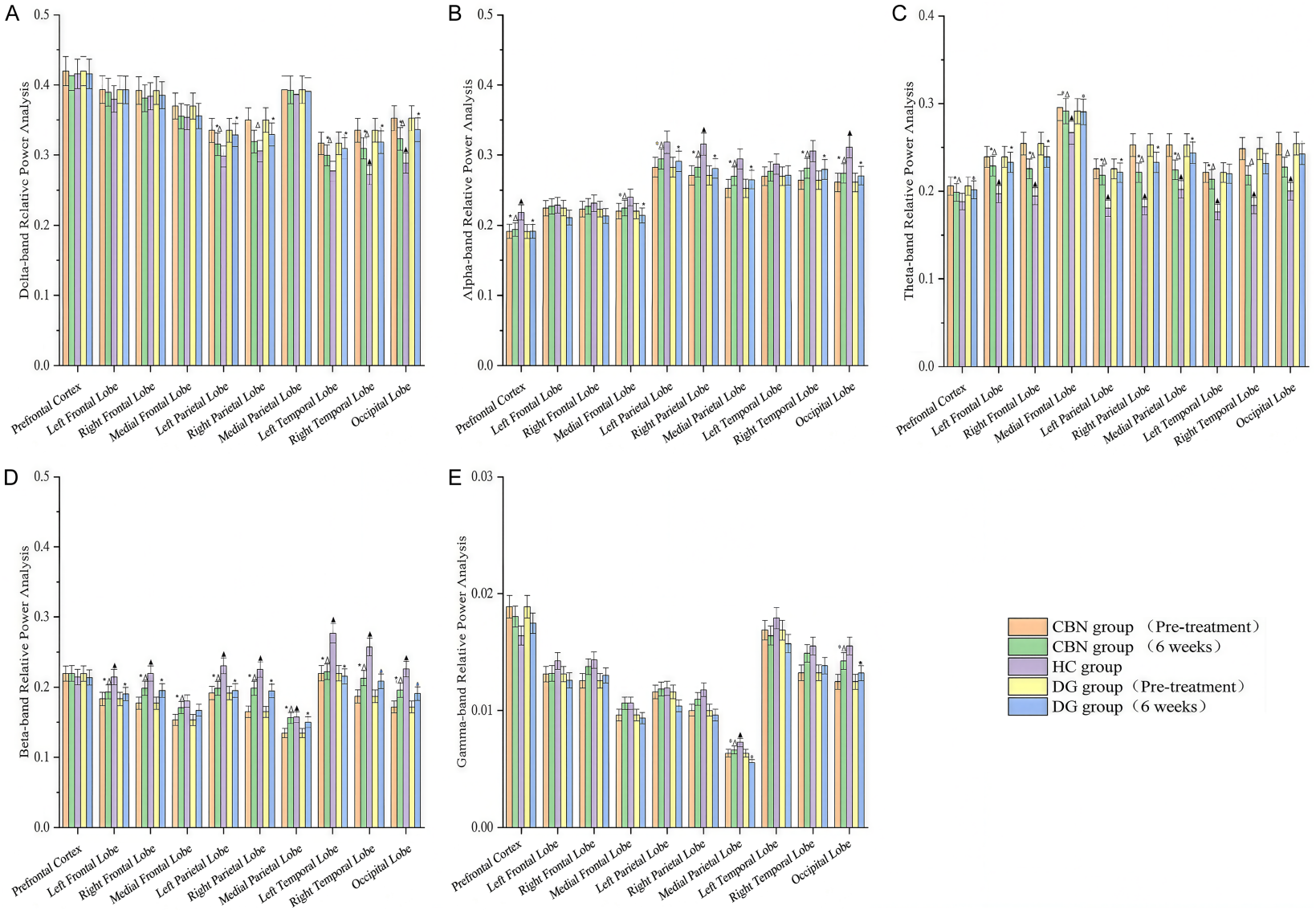

Figure 4. Relative power analysis. A: Delta-band; B: Alpha-band; C: Theta-band; D: Beta-band; E: Gamma-band. Statistical significance symbols: ▲ indicates CBN vs HC (P<0.05), △ indicates DG vs HC (P<0.05), * indicates CBN vs DG (P<0.05). Symbols are placed above the bars of the corresponding group to indicate the comparison.

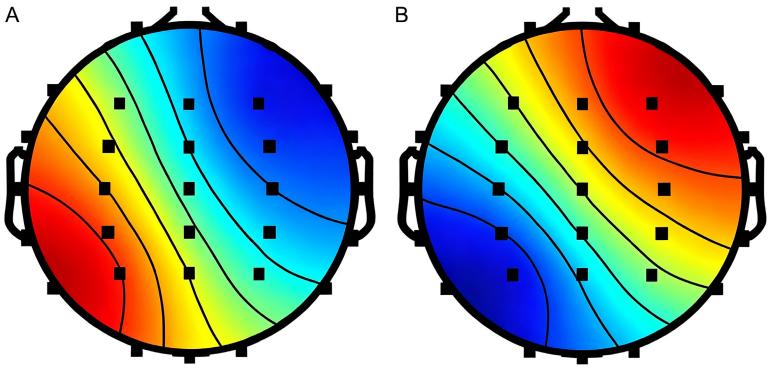

Figure 5. Representative scalp topographic maps of relative power changes. A: Pre-CBN treatment; B: Post-CBN treatment.

SF-36 scores, beneficial changes in articular cartilage morphology, and decreases in joint effusion and synovial thickness. In addition, CBN showed superior improvements in several clinical and imaging parameters compared with celecoxib treatment. These findings are consistent with previous randomized controlled evidence reported by Sun et al. [27], which demonstrated that acupuncture-based interventions can significantly improve pain and functional outcomes in KOA patients, further supporting the clinical utility of acupuncture-based interventions for this condition.

miRNAs are small non-coding RNA molecules that regulate gene expression post-transcriptionally by binding to target mRNAs, leading to mRNA degradation or translational repression. Through these regulatory mechanisms, miRNAs participate in diverse biological processes, including cell growth, differentiation, apoptosis, and disease progression. In articular cartilage, miRNAs are involved in chondrocyte homeostasis and the regulation of cartilage degeneration pathways [28, 29]. Consistent with the above analysis, CBN therapy significantly increased miR-140 levels and decreased miR-30 levels in both blood plasma and synovial fluid of KOA patients. In addition, these regulatory effects more pronounced in the CBN group than in the celecoxib group. These findings suggest that CBN may exert therapeutic effects in KOA partly through modulation of OA-associated miRNA profiles.

KOA is characterized by chronic low-grade inflammation within the joint microenvironment. Damage to the articular cartilage activation of synovial tissues can promote the release of inflammatory factors, further amplifying inflammatory responses and pain sensitization [30]. In this study, CBN treatment effectively reduced synovial fluid levels of IL-1β and TNF-α compared with baseline values and the celecoxib group. IL-1β is a key inflammatory cytokine involved in OA progression and can promote synovial activation and cartilage matrix degradation [31, 32]. TNF-α contributes to inflammatory responses by regulating osteoblast activity, osteoclastogenesis, and production of mononuclear granulocyte-stimulating factor [33, 34]. The interaction between IL-1β and TNF-α activates inflammatory signaling cascades, promotes the release of chemokines and adhesion molecules, and thus aggravates cartilage degradation and joint pain [35, 36].

EEG offers millisecond-level temporal resolution for assessing clinical brain functional imaging and is particularly suitable for investigating dynamic neural responses associated with acupuncture and chronic pain processing. In this study, significant differences in resting-state EEG relative power were observed after treatment in both the CBN and DG groups. Before treatment, the CBN and DG groups showed certain differences from the HC group in the Theta and Beta bands, with more prominent abnormalities observed in Theta band. Increased Theta activity has been reported in various pathological conditions, including inflammation, neurological injury, and cerebrovascular disease [37].

Chronic pain may shift brain activity toward lower-frequency theta waves; a reduction in theta power following treatment may indicate enhanced pain-coping mechanisms. Beta oscillations are generally associated with cortical arousal, sensorimotor processing, and cognitive engagement during wakefulness. Alterations in Beta activity may reflect changes in cortical excitability and attentional processing [38]. These results indicate that CBN therapy was more effective than the drug treatment in modulating neurophysiological activity.

Although EEG offers excellent temporal resolution and is suitable for brain network analysis,

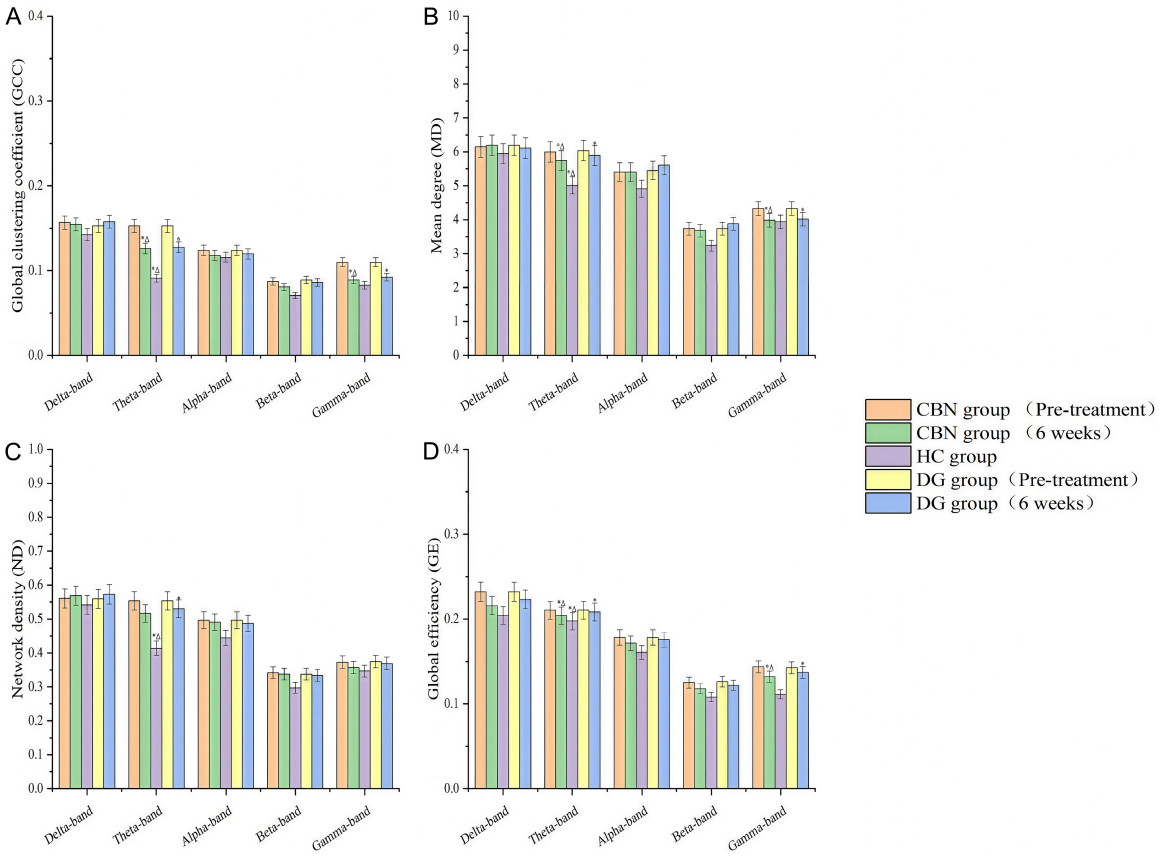

Figure 6. Brain network topological analysis. A: Global clustering coefficient (GCC); B: Mean degree (MD); C: Network density (ND); D: Global efficiency (GE). Statistical significance symbols: ▲ indicates CBN vs HC (P<0.05), △ indicates DG vs HC (P<0.05), * indicates CBN vs DG (P<0.05). Symbols are placed above the bars of the corresponding group to indicate the comparison.

Table 9. Spearman correlation analysis between Theta- and Gamma-band relative power in various brain regions and WOMAC scores in the CBN group

Brain Parcellation	WOMAC			
	Theta-band		Gamma-band	
	ρ-value	*P*-value	ρ-value	*P*-value
Prefrontal Cortex	0.21	0.285	-0.19	0.238
Left Frontal Lobe	0.37	0.037	-0.15	0.457
Right Frontal Lobe	0.28	0.124	-0.33	0.039
Medial Frontal Lobe	0.24	0.132	-0.14	0.524
Left Parietal Lobe	0.32	0.083	-0.19	0.316
Right Parietal Lobe	0.21	0.265	-0.16	0.525
Medial Parietal Lobe	0.21	0.133	-0.27	0.137
Left Temporal Lobe	0.19	0.323	-0.13	0.494
Right Temporal Lobe	0.22	0.232	-0.22	0.248
Occipital Lobe	0.19	0.296	-0.18	0.683

it spatial resolution is relatively limited compared to MRI. In this study, EEG combined with graph-theoretical analysis was to applied to characterize changes in functional brain network topology associated with CBN treatment in patients with KOA. At baseline, KOA patients exhibited abnormal enhancements in prefrontal functional connectivity within the Theta and Gamma bands compared with healthy controls. After treatment, these abnormal connectivity patterns significantly reduced. After treatment, both bands showed a significant change in the global clustering coefficient, average clustering coefficient and global efficiency of brain networks compared with the pre-treatment levels. These parame-

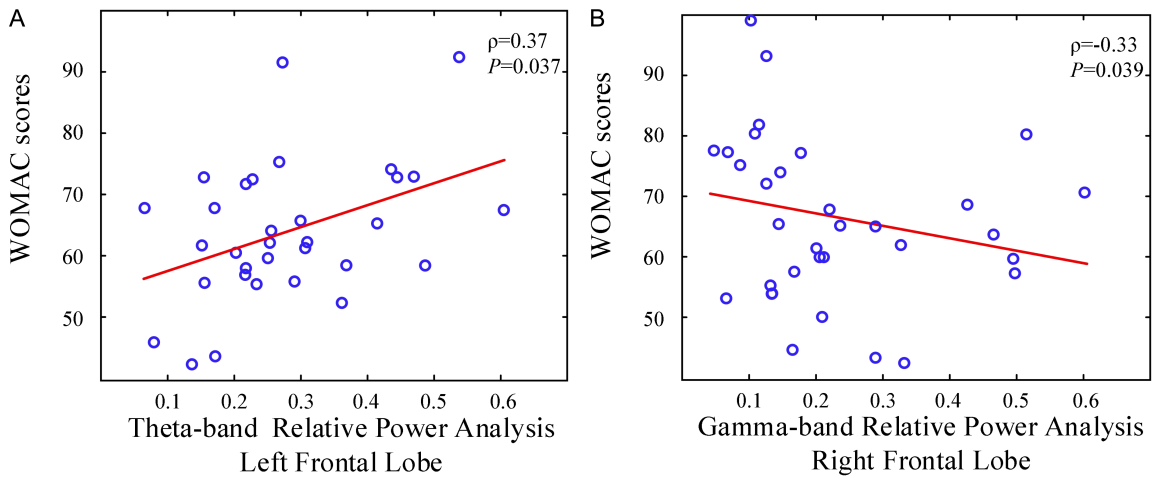

Figure 7. Correlation analysis. A: The Theta-band relative power in the left frontal region was positively correlated with the change in WOMAC score from baseline to post-treatment in the CBN group; B: The Gamma-band relative power in the right frontal region demonstrated a negative correlation with the change in WOMAC score after treatment.

ters shifted toward the levels observed in healthy control group, indicating that CBN may modulate abnormal functional network organization associated with KOA-related pain processing.

The medial prefrontal cortex (mPFC), located in the frontal lobe, is a key component of the default mode network and plays important roles in self-awareness and pain modulation. It modulates the descending pain pathway to process nociceptive stimuli in the spinal cord. Correlation analysis between EEG patterns and WOMAC scores revealed that Theta-band relative power in the left frontal region was positively correlated with changes in WOMAC scores, whereas Gamma-band relative power in the right frontal region showed a negative correlation with WOMAC score changes. These findings suggest that alterations in frontal cortical oscillatory activity may be associated with clinical improvement following CBN treatment.

Despite these strengths, several limitations should be acknowledged. First, the treatment protocol applied a fixed combination of acupoints, which precludes differentiation of the individual contributions of each point versus their combined effect. Second, only a relatively limited number of biomarkers (miR-140, miR-30, IL-1β, TNF-α) were investigated, and other potentially relevant molecular pathways were not assessed. Third, while CBN was associated with alterations in cortical oscillatory activity and prefrontal functional connectivity, the specific neural pathways through which acupuncture stimulation may influence peripheral inflammatory responses remain unknown. Additionally, the feedback loops between central nervous system modulation and synovial inflammation regulation have not been elucidated. Despite these limitations, this study establishes a novel multi-dimensional "brain-molecule-clinic" assessment system and demonstrates that CBN is an effective non-pharmacological treatment for KOA, acting through regulation of specific miRNAs and inflammatory cytokines, as well as normalization of aberrant brain activity and functional connectivity.

Conclusion

This randomized controlled trial demonstrates that CBN is an effective non-pharmacological intervention for knee osteoarthritis, showing superior efficacy over oral celecoxib in relieving symptoms, restoring joint structure, and enhancing quality of life. The therapeutic effects of CBN are mediated, at least in part, through upregulation of miR-140, downregulation of miR-30, reduction of inflammatory cytokines IL-1β and TNF-α, and normalization of aberrant brain oscillatory activity and prefrontal functional connectivity. The integrated "brain-molecule-clinic" framework proposed in this study provides a multi-dimensional approach for investigating the potential mechanisms of CBN in KOA. Further studies with larger sample sizes

and extended follow-up are warranted to validate these findings and explore the long-term efficacy of CBN.

Acknowledgements

This study was supported by the Youth Training and Excellence Project of Shaanxi Provincial Administration of Traditional Chinese Medicine (No. 2021-PY-008), and the Research Project of Shaanxi Provincial Administration of Traditional Chinese Medicine (No. SZY-KJCYC-2025-LC-004).

Disclosure of conflict of interest

None.

Address correspondence to: Yi Ren, Department of Rehabilitation Medicine, Hanzhong Hospital of Traditional Chinese Medicine, No. 8 Dongchang Street, Dahekan Town, Nanzheng District, Hanzhong 723102, Shaanxi, China. E-mail: renyionly@163.com

References

[1] Song M, Kim WJ, Shim J and Song K. Latilactobacillus sakei LB-P12 ameliorates osteoarthritis by reducing cartilage degradation and inflammation via regulation of NF-κB/HIF-2α pathway. J Microbiol Biotechnol 2025; 35: e2504013.

[2] Liu H, Qin L, Liu Y, Meng X, Li C and He M. Knee osteoarthritis rehabilitation: an integrated framework of exercise, nutrition, biomechanics, and physical therapist guidance-a narrative review. Eur J Med Res 2025; 30: 826.

[3] Yokota S, Ishizu H, Miyazaki T, Takahashi D, Iwasaki N and Shimizu T. Osteoporosis, osteoarthritis, and subchondral insufficiency fracture: recent insights. Biomedicines 2024; 12: 843.

[4] Song K, Hu J, Yang M, Xia Y, He C, Yang Y and Zhu S. Pulsed electromagnetic fields potentiate bone marrow mesenchymal stem cell chondrogenesis by regulating the Wnt/β-catenin signaling pathway. J Transl Med 2024; 22: 741.

[5] Zhang Y, Chen Z, Cheng Y, Zhou Y, Yang Y, Che M, Zhang Y and Li Y. Puerarin attenuates osteoarthritis via multi-target regulation of inflammation, apoptosis, and ECM degradation. J Cell Mol Med 2025; 29: e70833.

[6] Jin X, Yu Y, Lin Y, Yang J and Chen Z. Tendon-regulating and bone-setting manipulation promotes the recovery of synovial inflammation in rabbits with knee osteoarthritis via the TLR4-MyD88-NF-κB signaling pathway. Ann Transl Med 2023; 11: 245.

[7] Wang W, Jiang T, Zhang J, Liu J, Chan LC, Lin M, Li J, Ding C, Chiu KY, Fu H, Chan PK and Wen C. Subchondral bone expansion in advanced knee osteoarthritis: relation with radiographic severity and role in surgical decision-making. Osteoarthr Cartil Open 2024; 6: 100461.

[8] Lindberg V and Baak J. The majority of Norwegian patients with treatment-resistant chronic pain regained normal national health standards within 12 months after De-Qi acupuncture - a prospective observational propensity score matched study. Front Pain Res (Lausanne) 2025; 6: 1521466.

[9] Zeng L, Zhou G, Yang W and Liu J. Guidelines for the diagnosis and treatment of knee osteoarthritis with integrative medicine based on traditional Chinese medicine. Front Med (Lausanne) 2023; 10: 1260943.

[10] Chen H, Shi H, Gao S, Fang J, Yi J, Wu W, Liu X and Liu Z. Durable effects of acupuncture for knee osteoarthritis: a systematic review and meta-analysis. Curr Pain Headache Rep 2024; 28: 709-722.

[11] Mathew J, Adhia DB, Hall M, De Ridder D and Mani R. EEG-based cortical alterations in individuals with chronic knee pain secondary to osteoarthritis: a cross-sectional investigation. J Pain 2024; 25: 104429.

[12] Aae TF, Jakobsen RB, Dahl MB, Årøen A, Randsborg PH, Hoel MS and Lian ØB. Physical activity and diurnal variation have no impact on plasma microRNA-140 expression levels in patients with knee osteoarthritis and healthy controls. Osteoarthr Cartil Open 2025; 8: 100720.

[13] Jamshidi A, Espin-Garcia O, Wilson TG, Loveless I, Pelletier JP, Martel-Pelletier J and Ali SA. MicroRNA signature for early prediction of knee osteoarthritis structural progression using integrated machine and deep learning approaches. Osteoarthritis Cartilage 2025; 33: 330-340.

[14] Ren Y, Liu F, Zhang Y, Fu N, Xi X, Yang X and Li X. Effects of close-to-bone needling on expression of type-II collagen and markers in cartilage in rabbits with osteoarthritis of knee and imaging observation. Zhongguo Zhen Jiu 2016; 36: 622-628.

[15] Liu F, Li XZ, Fu NN, Xi XF, Ren Y, Yang XG and Zhang Y. Effect of eletroacupuncture with close-to-bone needling treatment on expression of Sox9, VEGF and ColX in impaired cartilage of rabbits with knee osteoarthritis. Nan Fang Yi Ke Da Xue Xue Bao 2016; 36: 997-1003.

[16] Fu NN, Li XZ, Yang XG, Liu F, Xi XF, Ren Y and Zhang Y. Effect of electroacupuncture with near-to-bone needling to chondrocyte apoptosis and proliferation on the knee osteoarthritis model. Sichuan Da Xue Xue Bao Yi Xue Ban 2016; 47: 708-713.
[17] Mei H, Wang J, Zheng X, Yan R, Li W, Wang P, Wang X and Liu L. Conjoint analysis of single-cell sequencing and high-throughput virtual screening regarding DDR2 in osteoarthritis disease models. Eur J Med Res 2025; 30: 954.
[18] Li X, Chen Y, Xu R, Wang Y, Jian F, Long H and Lai W. Delay in articular cartilage degeneration of the knee joint by the conditional removal of discoidin domain receptor 2 in a spontaneous mouse model of osteoarthritis. Ann Transl Med 2020; 8: 1178.
[19] MacPherson H, Altman DG, Hammerschlag R, Youping L, Taixiang W, White A and Moher D; STRICTA Revision Group. Revised STandards for reporting interventions in clinical trials of acupuncture (STRICTA): extending the CONSORT statement. J Altern Complement Med 2010; 16: ST1-14.
[20] Tan Y, Ma X, Wang Q, Zhao Z, Zhai W and Guo Y. Investigation for use of the name and location of acupoints(GB/T 12346-2006), national standard. Zhongguo Zhen Jiu 2016; 36: 871-874.
[21] Bellamy N, Wilson C and Hendrikz J. Population-based normative values for the Western Ontario and McMaster (WOMAC) osteoarthritis index: part I. Semin Arthritis Rheum 2011; 41: 139-148.
[22] Li JW, Xiang SY, Ma ZY, Feng YB, Tong HY, Geng HP, Jin J and Su X. Clinical observation on cake-separated mild-warm moxibustion for treatment of knee osteoarthritis. Zhongguo Zhen Jiu 2008; 28: 17-19.
[23] Zhang Y, Qu B, Lun SS, Guo Y and Liu J. The 36-item short form health survey: reliability and validity in Chinese medical students. Int J Med Sci 2012; 9: 521-526.
[24] Jiao J, Dong B, Han Y, Zheng Q and Lin X. Acupuncture in knee osteoarthritis: a narrative review of clinical efficacy and neuroimmune-endocrine mechanisms. J Pain Res 2025; 18: 4989-4998.
[25] Mei F, Yao M, Wang Y, Ma Y, Liu Y, Wu M, Wang Z, Feng L, Hu K and Ma B. Acupuncture for knee osteoarthritis: a systematic review and meta-analysis. J Evid Based Med 2023; 16: 138-140.
[26] Luo X, Liu J, Li Q, Zhao J, Hao Q, Zhao L, Chen Y, Yin P, Li L, Liang F and Sun X. Acupuncture for treatment of knee osteoarthritis: a clinical practice guideline. J Evid Based Med 2023; 16: 237-245.
[27] Sun J, Liang Y, Luo KT, Shao XM, Tu MQ, Wu XT, Liu F, Li XW, Chen YD, Zhang QF, Ji CH, Li RR, Li XY, Xu F and Fang JQ. Efficacy of different acupuncture techniques for pain and dysfunction in patients with knee osteoarthritis: a randomized controlled trial. Pain Ther 2025; 14: 737-751.
[28] Wang Z, Zheng X, Lin J, Zhou B, Zeng Z, Gao H, Chen H and Tang C. Electroacupuncture ameliorates cartilage damage in a rat model of knee osteoarthritis and regulates expression of miRNAs and the TLR4/NF-κB pathway. Acupunct Med 2025; 43: 164-173.
[29] Li S, Peng Y, Yu Y, Xu H, Yin Z, Du Y, Ma M, Ji Z and Qian W. Investigating the impact of circulating MicroRNAs on knee and hip osteoarthritis: causal links, biological mechanisms, and drug interactions. Int J Mol Sci 2024; 26: 283.
[30] Fan Y, Bian X, Meng X, Li L, Fu L, Zhang Y, Wang L, Zhang Y, Gao D, Guo X, Lammi MJ, Peng G and Sun S. Unveiling inflammatory and prehypertrophic cell populations as key contributors to knee cartilage degeneration in osteoarthritis using multi-omics data integration. Ann Rheum Dis 2024; 83: 926-944.
[31] Qiao J, Guo X, Zhang L, Zhao H and He X. Autologous platelet rich plasma injection can be effective in the management of osteoarthritis of the knee: impact on IL-1 β, TNF-α, hs-CRP. J Orthop Surg Res 2024; 19: 703.
[32] Liu T, Lian Q, Zeng Y, Que B, Tang Y, Wu W and Qiu R. Clinical efficacy of fire-needle warming therapy in the treatment of knee osteoarthritis of cold-dampness type and its effect on serum IL-1β and MMP-3. Clin Rheumatol 2025; 44: 3003-3011.
[33] Zhai S, Wu R, Fan S, Du G, Zhao X, Wan H and Huang W. Screening of TNF signaling pathway-related genes in knee osteoarthritis (KOA) using WGCNA and machine learning. Medicine (Baltimore) 2025; 104: e43849.
[34] Shao Z, Wang T, Yan X, Ning R, Xu X, He Q, Zhang X, Jiang M and Yang C. Identification of a RANKL/TNF-α dual-inhibitor as a potential disease-modifying agent for the treatment of knee osteoarthritis. J Med Chem 2025; 68: 10216-10237.
[35] Zhang J, Li K and Qiu X. Exploring causal correlations between inflammatory cytokines and knee osteoarthritis: a two-sample Mendelian randomization. Front Immunol 2024; 15: 1362012.
[36] Raut RD, Chakraborty AK, Neogi T, Albro M, Snyder B, Schaer TP, Zhang C, Grinstaff MW and Bais MV. A multi-tissue human knee single-cell atlas identifies that osteoarthritis reduces regenerative tissue stem cells while increasing inflammatory pain macrophages. Commun Biol 2025; 8: 1146.

[37] Zhao S, Alhumaid MM, Li H, Wei X, Chen SS, Jiang H, Gong Y, Gu Y and Qin H. Exploring the effects of sleep deprivation on physical performance: an EEG study in the context of high-intensity endurance. Sports Med Open 2025; 11: 4.

[38] Ren Y, Wu H, Li W, Zeng Q and Liu Y. Central mechanism of the short-needling method for treating knee osteoarthritis based on EEG signals. Zhongguo Zhen Jiu 2026; 46: 29-38.